VIII International Conference on Computational Methods for Coupled Problems in Science and Engineering
COUPLED PROBLEMS 2019
E. Oñate, M. Papadrakakis and B. Schrefler (Eds)

FLUID-STRUCTURE INTERACTION AND HOMOGENIZATION: FROM SPATIAL AVERAGING TO CONTINUOUS WAVELET TRANSFORM

S. MOKHTARI[*,a], G. RICCIARDI[a], V. FAUCHER[b], P. ARGOUL[c] and L.ADELAIDE[c]

[a]CEA Cadarache, DEN/DTN/STCP/LTHC
13115 Saint-Paul-Lez-Durance, France

[b]CEA Cadarache, DEN/DTN
13115 Saint-Paul-Lez-Durance, France

[c]IFSTTAR, MAST/EMGCU
14-20 boulevard Newton, 77447 Marne-la-Vallée Cedex 2, France

Key words: fluid-structure interaction, compressible flow, spatial filtering, multi-scale, homogenization, wavelets.

1 INTRODUCTION

Fluid-structure interaction (FSI) is classicaly modeled according a separated and local approach. It enables to take full advantage of the numerical methods specifically designed for each medium. However, it requires to take great care of the interface, and to exchange, between the algorithms, the information related to boundary conditions [1]. This treatment of the interface can quickly become too cumbersome in complex flow geometries, as in the industrial case study driving this work: an inviscid compressible flow interacting with French PWR fuel assemblies (Fig. 1a).

In such specific applications, where the solid medium exhibits a discontinuous but periodic design, an homogenized and global approach is preferred [2]. Inspired by porous media [3, 4], multiphase flows, or Large Eddy Simulation (LES), it relies on a spatial averaging of the balance equations, thus allowing to remove all interfaces. However, such filtering techniques exhibit two major limitations: first, they do not deal properly with boundary conditions, due to the non-commutativity between the filtering operator and spatial derivatives, as detailed in [5, 6, 7] for LES; second, filtering implies loss of microscopic information, and thus requires a closure model to describe interactions between resolved and unresolved scales.

In order to bypass these limitations, and especially tackle the multi-scale issue of closure, the authors hereafter put forward a new formalism to homogenize the fluid and solid media : continuous wavelet transform (CWT). Indeed, once applied to each medium balance equations, CWT allows to robustly derive a system of filtered and homogenized PDEs, while travelling back and forth between resolved and unresolved scales, thanks to its ability to reconstruct a signal from its wavelet coefficients.

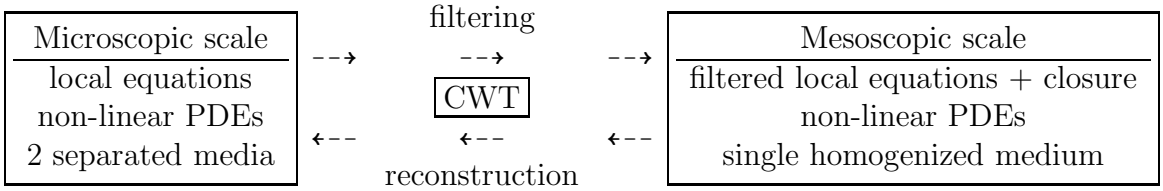

In literature, wavelets have been extensively used, for a couple decades now, in signal processing and modal identification [8], and also for the numerical computation of PDEs [9, 10, 11, 12, 13]. Nevertheless, to the authors' knowledge, wavelets are in most cases used with the "discrete (orthogonal) wavelet transform" (DWT) formalism, and under the assumption that the signal is known at the microscopic scale (signal processing, coarsening of a fine grid). The reference work of [14] stands among the rare examples of the use of CWT on linear differential equations, in order to derive algebraic equations.

In the current work, wavelets are used to derive filtered and homogenized equations on continuum fields, in the sense of continuum mechanics. CWT is therefore more relevant than DWT. The thorough description of the filtering process, and the numerical resolution of the filtered equations, exceed the scope of the current work. However, it can here be noted that CWT will be implemented in a 2D formalism, as the solid medium exhibits a periodic design along the transverse directions only (Fig. 1a). Moreover, the authors hereafter focus on the fluid, and consider the solid medium as a fixed and rigid body, only acting as a boundary condition for the flow. The structure displacement and deformation will be considered in further developments.

The following of the present article is hereafter divided into five parts. First, the fluid physical and mathematical modeling are described, after a brief overview of the solid medium. Second, the wavelet-based multi-scale modeling is introduced : some key points on CWT are recalled, followed by the choice of the analyzing wavelet. Third, the filtered equations are displayed, thus highlighting the key issues of closure and microscopic reconstruction. Fourth, this modeling is confronted with a 2D numerical case study, consisting in the propagation of a transverse pressure wave through rod bundles, for which a reference solution is computed with EUROPLEXUS software. These preliminary numerical investigations aim to bring a first light on the CWT ability to reconstruct the force applied by the fluid on the micro-structure. Finally, the last section is dedicated to a conclusion.

2 Physical and mathematical modeling

2.1 Solid medium

In the industrial case study, the solid medium is composed of fuel assemblies used in a French PWR. As shown in Fig. 1a, they exhibit a discontinuous but periodic design, with a beam-like geometry (20 $cm^2 \times 4$ m). A French 900 MW PWR possesses 157 fuel assemblies, each composed of 264 fuel rods (5 mm radius), 5 instrumentation guide thimbles, and 24 control rod guide thimbles. The latter bring stiffness and cohesion to the structure thanks to 8 spacer grids (Fig. 1b) placed along the assembly. The reader can refer to [2] for further details on the design and mechanical behavior of PWR fuel assemblies.

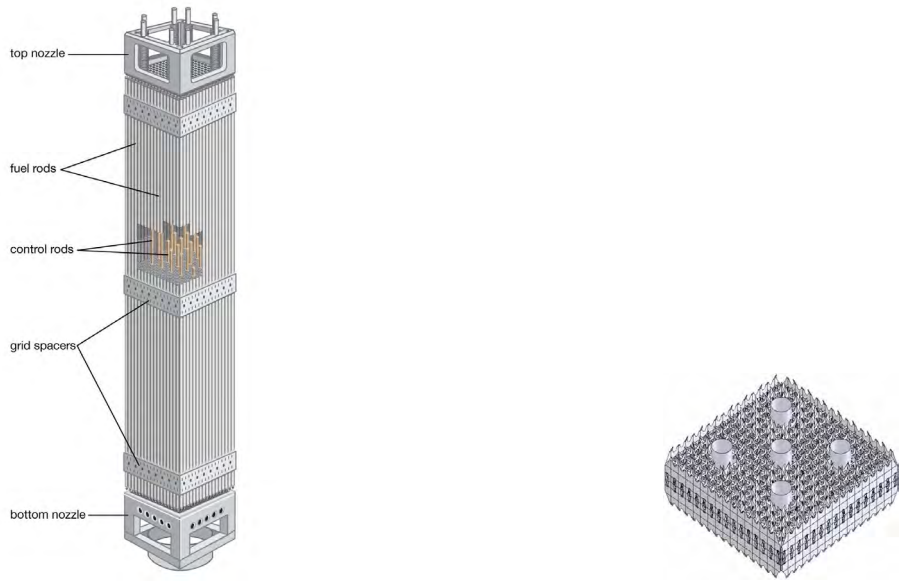

(a) (b)

Figure 1: PWR fuel assemblies design: fuel assembly (a) and spacer grid (b).

2.2 Fluid

Under nominal operating conditions, the (liquid) water flow interacting with PWR fuel assemblies is almost vertical, incompressible and very turbulent, with a Reynolds number around 10^5, at around 300 degrees Celsius and 155 bar. For this study, a fast transient compressible flow is considered, with the following modeling framework:

- monophasic compressible flow;
- inviscid fluid;

- kinetic turbulent energy, gravity effects and superficial tension are negligible compared to pressure gradients;
- conduction heat transfer is negligible;
- barotropic state law;

2.3 Local equations

The water flow is thus driven by the following Euler compressible equations:

$$\begin{array}{rcll} \partial_t \rho + div\left(\rho \underline{v}\right) & = & 0 & \text{in } \Omega_f, \\ \partial_t \left(\rho \underline{v}\right) + div\left(\rho \underline{v} \otimes \underline{v}\right) & = & -\underline{\nabla}\, p & \text{in } \Omega_f, \\ \partial_t \left(\rho e\right) + div\left(\left(\rho e + p\right) \underline{v}\right) & = & 0 & \text{in } \Omega_f, \end{array} \tag{1}$$

which translate respectively the conservation of mass, momentum and energy.

This system of conservation laws is closed by a barotropic state law:

$$p = p_{ref} + c^2 \left(\rho - \rho_{ref}\right), \tag{2}$$

where ρ_{ref} and p_{ref} are respectively a reference density and pressure, and $c = \sqrt{\partial_\rho p}$ the sound velocity in the fluid.

As for the boundary conditions, the assumption of inviscid fluid here implies:

$$\underline{v} \cdot \underline{n} \;=\; 0 \quad \text{on } \partial\Omega_f, \tag{3}$$

where $\underline{n}$ is the outward unit normal vector on the boundary $\partial\Omega_f$.

Given an initial data, the mathematical problem is thus well-posed. The fluid physical and mathematical modeling being stated, the following section can now introduce the multi-scale and homogenized modeling.

3 A multi-scale and homogenized modeling: from spatial averaging to CWT

Considering the lack of smoothness of some of the fields present in (1) (the pressure gradient and divergence operators are only defined in a distributional sense), a plain volume averaging of the equations is not mathematically robust. Moreover, a classical convolution product, as used in LES, does not enable to connect resolved and unresolved scales, and to reconstruct the force applied on the micro-structure. Continuous wavelet transform (CWT), conversely, fulfill these requirements.

In the following subsections, some key points on CWT are first recalled. The choice of the analysing wavelet is then motivated.

3.1 Continuous wavelet transform : definition and properties

Wavelets were first introduced as a tool for time-frequency analysis, in a 1D formalism. From an analyzing wavelet Ψ, classicaly defined as an oscillating function with a well-localized time-support, and a band-pass behavior $\left(\omega_{\Psi}, \Delta\omega_{\Psi}\right)$ in the Fourier domain, two parameters enable to build a familiy of translated ($u \in \mathbb{R}$) and dilated ($s > 0$) wavelets:

$$\Psi_{s,u}(t) = \frac{1}{\sqrt{s}}\Psi\left(\frac{t-u}{s}\right) \tag{4}$$

The resulting wavelet family $\left(\Psi_s\right)_{s>0}$ also exhibits a band-pass behavior. The interested reader can refer to [8, 15] for further details on wavelets and time-frequency analysis. Hereafter, wavelets are used as a spatial filtering tool. The above definition (4) is then generalized by adding one (respectively two) angular parameter(s) θ (resp. θ/φ) in 2D (resp. in 3D). In the following, $d = 2$.

Definition: continuous wavelet transform (2D) *Assume $\Psi \in L^1\left(\mathbb{R}^d\right) \cap L^2\left(\mathbb{R}^d\right)$, with real or complex values, and satisfying a zero average condition:*

$$\int_{\mathbb{R}^d} \Psi(\underline{x})\ \mathrm{d}\underline{x} = 0. \tag{5}$$

The continuous wavelet transform of a finite-energy signal $f \in L^2\left(\mathbb{R}^d\right)$ is defined as:

for all positions $\underline{u} \in \mathbb{R}^d$, scales $s > 0$, and angle $\theta \in [0, 2\pi[$:

$$\mathcal{W}[f](s, \underline{u}, \theta) = \frac{1}{\sqrt{s}^d}\int_{\mathbb{R}^d} f(\underline{x})\Psi\left(\left(\underline{\underline{R_\theta}}\right)^{-1}\frac{\underline{x}-\underline{u}}{s}\right)^*\ \mathrm{d}\underline{x}\ \text{(in 2D)}, \tag{6}$$

where:

- $\mathcal{W}[f](s, \underline{u}, \theta)$ is the wavelet coefficient;
- *Ψ is the analyzing wavelet, and Ψ^* its complex conjugate;*
- $\underline{\underline{R_\theta}} = \begin{pmatrix}\cos(\theta) & -\sin(\theta)\\ \sin(\theta) & \cos(\theta)\end{pmatrix}_{\left(\underline{e_1},\underline{e_2}\right)}$ *is the 2D rotation matrix with respect to the $\left(O, \underline{e_1} \wedge \underline{e_2}\right)$ axis, where $\left(\underline{e_1}, \underline{e_2}\right)$ is the orthonormal cartesian basis of $\mathbb{R}^2$;*

If $d = 1$, the θ variable and the rotation matrix $\underline{\underline{R_\theta}}$ are omitted.

Thus, CWT can either be seen as a scalar or convolution product, between a signal and a wavelet family. But more importantly, CWT allows to reconstruct a signal at the

microscopic scale from its wavelet coefficients, assuming the analyzing wavelet satisfies the following admissibility condition (where $\mathcal{F}$ denotes the Fourier transform):

$$C_\Psi = \int_{\mathbb{R}^2} \frac{\left|\mathcal{F}[\Psi]\left(\underline{k}\right)\right|^2}{\left\|\underline{k}\right\|^2} \, \mathrm{d}\underline{k} < +\infty \text{ (in 2D)}. \tag{7}$$

For further details on this property, the reader can refer to the reference book of [15]. Let us now detail the choice of the analyzing wavelet.

3.2 Analyzing wavelet

In literature, two major wavelet families are available: complex analytic and directional wavelets, versus real isotropic wavelets. In this work, the latter are better suited to "observe" pressure waves propagating in different directions simultaneously. The mexican hat (Fig. 2) has thus kept our attention. Its definition is recalled below (8) :

$$\forall \underline{k} \in \mathbb{R}^2, \, \mathcal{F}[\Psi](\underline{k}) = 4\sigma^3\sqrt{2\pi}\left\|\underline{k}\right\|^2 e^{-\frac{\sigma^2\left\|\underline{k}\right\|^2}{2}} \text{ (in 2D)}. \tag{8}$$

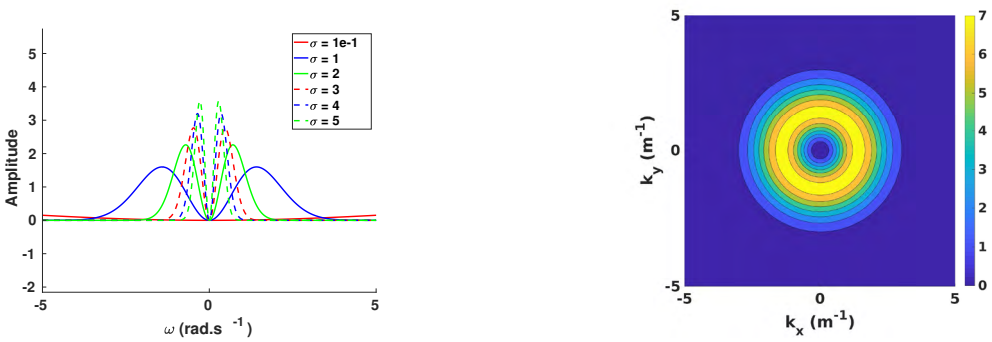

(a) (b)

Figure 2: 1D (a) and 2D (b, $\sigma = 1$) mexican hat Fourier transforms.

This wavelet exhibits a band-pass behavior in the Fourier domain, with a low selectivity. Besides, it satisfies the admissibility condition (7), with

$$C_\Psi = 32\pi^2\sigma^2 \text{ (in 2D)}. \tag{9}$$

The mexican hat thus allows to tackle the closure issue, as detailed in the following section.

4 Filtered equations: closure and microscopic reconstruction

The wavelet-based multi-scale modeling here introduced leads to the following filtered equations on $(\mathcal{W}[\rho], \mathcal{W}[\rho\underline{v}], \mathcal{W}[\rho e])$ (here in 3D for the sake of generality):

consider $T > 0$, for all $t \in [0, T[$, $s > 0$, and $\underline{u} \in \mathbb{R}^3$:

$$\begin{array}{rcl} \partial_t \mathcal{W}[\rho](s,\underline{u},t) + div\left(\mathcal{W}[\rho\underline{v}]\right)(s,\underline{u},t) & = & 0, \\ \partial_t \mathcal{W}[\rho\underline{v}](s,\underline{u},t) + div\left(\mathcal{W}[\rho\underline{v}\otimes\underline{v}]\right)(s,\underline{u},t) & = & -\underline{\nabla}\mathcal{W}[p](s,\underline{u},t) + \widehat{\underline{F_{S\to F}}}(s,\underline{u},t), \\ \partial_t \mathcal{W}[\rho e](s,\underline{u},t) + div\left(\mathcal{W}[(\rho e+p)\underline{v}]\right)(s,\underline{u},t) & = & 0, \end{array} \tag{10}$$

where

$$\widehat{\underline{F_{S\to F}}}(s,\underline{u},t) = -\int_{\partial\Omega_f} \widetilde{\Psi_s}^*(\underline{u}-\underline{\sigma}) p(\underline{\sigma},t)\underline{n}(\underline{\sigma})\,\mathrm{d}\underline{\sigma} \tag{11}$$

is a body force per unit of volume, now defined accross the whole space $\mathbb{R}^3$. In (11), the notation $\widetilde{\Psi}_s(\underline{x})$ refers to $\frac{1}{\sqrt{s}^d}\Psi(-\underline{x})$. As one can notice, this filtered body force exhibits the microscopic pressure on the fluid-structure interfaces. Thanks to the CWT formalism, it is now possible to link this unresolved pressure to its resolved counterpart, i.e. the wavelet coefficients $\mathcal{W}[p](s,\cdot,\cdot)$, and then to the density wavelet coefficients. Indeed, the filtering of the state law results in:

$$\forall t \in [0,T[,\ s>0,\ \underline{u}\in\mathbb{R}^3,\ \mathcal{W}[p](s,\underline{u},t) = c^2\mathcal{W}[\rho](s,\underline{u},t). \tag{12}$$

Nevertheless, such a solution to the closure issue exhibits two limitations. First, for the microscopic reconstruction to be exact, all wavelet coefficients, for all scales $s > 0$, are required. The key issue is thus to assess whether or not a limited number of resolved scales can provide a satisfactory approximation of the microscopic field. Second, this need of possibly numerous scales to assess the filtered body force (11) uncover an interdependence between the different scales: when solving the filtered equations for a specific scale s_i, one shall thus need the information related to other scales s_j. This fact will impact the design of the numerical methods for the filtered equations (10).

In academic cases, where the solution can be computed at the microscopic scale, criteria can be introduced in order to make an "optimal" choice between the precision of the reconstruction, and the computation cost. In the following, a mechanical criterion is put forward, based on the force applied by the fluid on the micro-structure:

$$\underline{F_{F\to S}}(t) = \int_{\partial\Omega_s} p(\underline{\sigma},t)\underline{n}(\underline{\sigma})\,\mathrm{d}\underline{\sigma}, \tag{13}$$

$$\left(\underline{F_{F\to S}}\right)_{N_s}(t) = \int_{\partial\Omega_s} p_{N_s}(\underline{\sigma},t)\underline{n}(\underline{\sigma})\,\mathrm{d}\underline{\sigma}, \tag{14}$$

where (14) is an approximation obtained by partially reconstructing the microscopic pressure field p with N_s scales on the range $[s_1, s_{N_s}]$.

To bring a first light on the CWT ability to recover the microscopic information with a limited number of resolved scales, the above criterion is applied on a 2D numerical case study, where the microscopic pressure field is computed with a validated code.

5 Numerical tests

This case study consists in a 2D transverse pressure wave propagating through a periodic solid medium, composed of 10×10 rods, as described in Fig. 3 and Tab. 1:

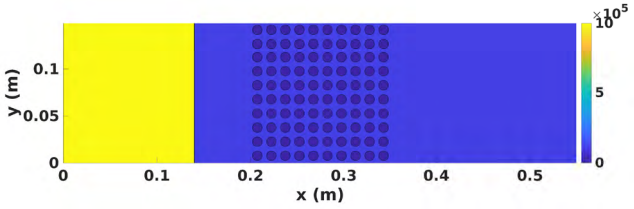

Figure 3: Geometry and initial loading : 10 bar (yellow) and 1 bar (blue).

X-dimension	Y-dimension	rods radius	Nb. of rods	rods position
0.55 m	0.15 m	5.10^{-3} m	10×10	$[20.25\text{ cm}, 35.25\text{ cm}]$

Table 1: Dimensions

The fluid barotropic state law and the structure behavior, here assumed homogeneous, isotropic, and linear elastic, are detailed in Tab. 2-3:

Reference density	Reference pressure	Sound velocity
$\rho_{ref} = 1000$ kg.m^{-3}	$p_{ref} = 10^5$ Pa	$c = 1300$ m.s^{-1}

Table 2: Fluid parameters

Young modulus	Poisson coefficient
$E = 210$ GPa	$\nu = 0.3$

Table 3: Rods parameters

The simulation of this case study is conducted with EUROPLEXUS software, a fast-transient dynamics code for fluids and structures. 3-noded triangle finite elements are used for the solid medium, while a cell-centered finite volume scheme is used for the fluid. The time discretization relies on an Euler explicit scheme. The resulting pressure field (Fig. 4) will be the reference for the mechanical criterion.

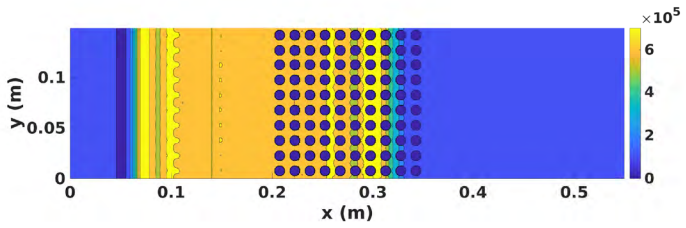

Figure 4: Pressure field (Pa) - time $= 1.6 \times 10^{-4}$ s.

Considering the micro-structure geometry and the reference pressure field (Fig. 4), wavelengths around 10^{-3} m, 10^{-4} m, and smaller (because of the rods boundaries) are expected to convey a significant part of the pressure field information.

The following figure (Fig. 5) shows the evolution of the force ratio (in the horizontal direction) with the number of computed scales N_s, and for standard deviations $\sigma \in \{10^{-2}, 10^{-1}, 1\}$. Two scale ranges are considered: $s\sigma \in [10^{-5}, 5.10^{-4}]$ and $s\sigma \in [10^{-5}, 10^{-3}]$. Moreover, the scale discretization δs is uniform. As can be expected, it appears that the larger range provides a better precision: the relative error indeed decreases from around 8% to 2%. Moreover, it can be noticed that, beyond the value $N_s = 10$, the number of computed scales does not have a significant impact on the reconstruction. However, a decrease to $N_s = 5$ scales has a visible influence, especially on the range

$s\sigma \in [10^{-5}, 10^{-3}]$. Finally, a decrease in the standard deviation σ does not impact the reconstruction. This confirms that σ has a very weak impact on the wavelet selectivity.

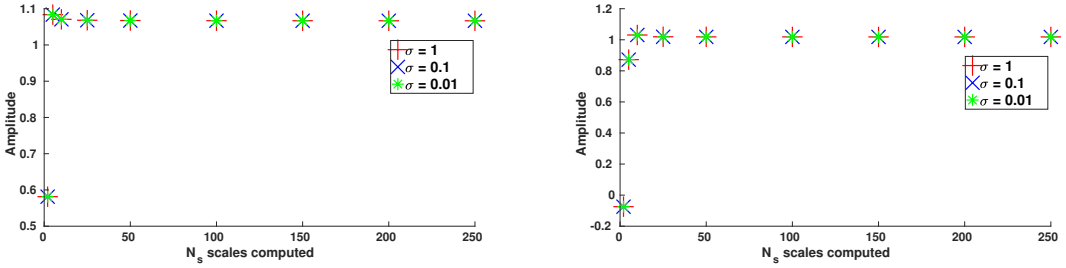

(a) $s\sigma \in [10^{-5}, 5.10^{-4}]$ (b) $s\sigma \in [10^{-5}, 10^{-3}]$

Figure 5: Force ratio - $\sigma \in \{10^{-2}, 10^{-1}, 1\}$ - time $= 8.10^{-5}$ s.

Thus, the mechanical criterion leads to the conclusion that $N_s = 10$ computed scales, on the range $s\sigma \in [10^{-5}, 10^{-3}]$, allow to recover the force applied on the micro-structure with a relative error of 2%. The corresponding wavelength range is detailed in Tab. 4:

Wavelength range	
$\sigma = 10^{-2}$ and $s \in [10^{-3}, 10^{-1}]$	
$\lambda_{min} \approx 2.45 \times 10^{-5}$ m	$\lambda_{max} \approx 6.55 \times 10^{-3}$ m

Table 4: Relevant wavelength range with respect to the mechanical criterion.

This range is consistant with the a priori estimation. In order to reduce this range, and especially increase λ_{min}, which will drive the mesh size for the filtered equations, one should get rid of the smallest scales in the range $s\sigma \in [10^{-5}, 10^{-3}]$. However, this would inevitably damage the precision of the reconstruction. For the sake of completeness, the following figure (Fig. 6) displays a zoom on the original and reconstructed pressure fields, with $\sigma = 10^{-2}$, $s \in [10^{-3}, 10^{-1}]$ and $N_s = 10$ computed scales.

6 Conclusion

A new homogenization formalism, based on continuous wavelet transform, was here promoted, in the context of a fast transient FSI between an inviscid compressible flow and a periodic solid medium. It allowed to robustly derive filtered and homogenized equations, and to connect resolved and unresolved scales without relying on any model. First promising results were highlighted for a 2D transverse pressure wave propagating through 10×10 rods, where the mexican hat wavelet showed its ability to reconstruct the force applied by the fluid on the micro-structure, with a limited number of computed scales.

In further developments, the focus shall be put on the derivation process of the filtered

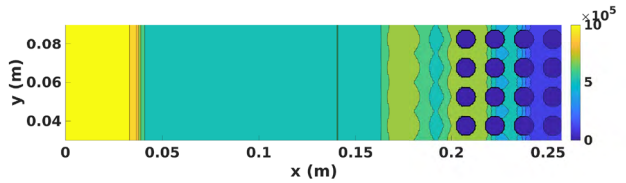

(a)

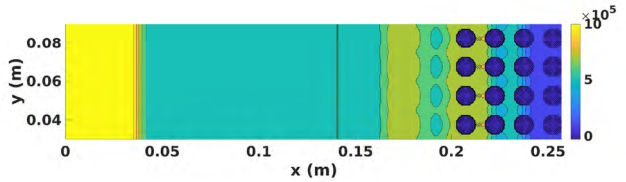

(b)

Figure 6: Original (a) and reconstructed (b) pressure (Pa) - $s\sigma \in [10^{-5}, 10^{-3}]$ - $N_s = 10$.

equations, and their numerical resolution. Moreover, both the deformation and displacement of the structure shall be taken into account in the local equations.

Finally, in a will to broaden the context of the present article, this multi-scale modeling can be linked to the wide and transverse topics of reduced order modeling and sparse representation of information. This work could indeed be extended to numerous physics and engineering branches, such as multiphase and turbulent flows, porous media, or heterogeneous materials for instance. However, this modeling can only be relevant if the fields of interest exhibit well-localized spectrum. Otherwise, the computation cost required for the resolution of the filtered equations, and the microscopic reconstruction, could be equivalent to direct numerical simulation.

REFERENCES

[1] Faucher, V., Crouzet, F. and Debaud, F. Mechanical consequences of LOCA in PWR : full scale coupled 1D/3D simulations with fluid-structure interaction. *Nuclear Engineering and Design.* (2014) **270**:359-378.

[2] Ricciardi, G., Bellizi, S., Collard, B. and Cochelin, B. Row of fuel assemblies analysis under seismic loading: modelling and experimental validation. *Nuclear Engineering and Design.* (2009) **239**:2692-2704.

[3] Robbe, M.-F. and Bliard, F. A porosity method to describe the influence of internal structures on a fluid flow in case of fast dynamics problems. *Nuclear Engineering and Design.* (2002) **215**:217-242.

[4] Chandesris, M., Serre, G. and Sagaut, P. A macroscopic turbulence model for flow in porous media suited for channel, pipe and rod bundles. *International Journal of Heat and Mass Transfer.* (2006) **49**:2739-2750.

[5] Ghosal, S. and Moin, P. The basic equations for the Large Eddy Simulation of turbulent flows in complex geometry. *Journal of Computational Physics.* (1995) **118**:24-37.

[6] Fureby, C. and Tabor, G. Mathematical and physical constraints on Large-Eddy Simulations. *Theoretical and Computational Fluid Dynamics.* (1997) **9**:85-102.

[7] Dunca, A., John, V. and Layton, W. J. The commutation errors of the space averaged Navier-Stokes equations on a bounded domain. *Journal of Mathematical Fluids Mechanics.* (2003) **20**:1-27.

[8] Le, T.-P. and Argoul, P. Continuous wavelet transform for modal identification using free decay response. *Journal of Sound and Vibration.* (2004) **277**:73-100.

[9] Jaffard, S. *Wavelets and analysis of partial differential equations.* NATO ASI Series, in Probabilistic and Stochastic Methods in Analysis, with applications (1991).

[10] Frohlich, J. and Schneider, K. An adaptive wavelet-vaguelette algorithm for the solution of PDEs. *Journal of Computational Physics.* (1997) **130**:174-190.

[11] Mallat, S. A theory for multiresolution signal decomposition: the wavelet representation. *IEEE Transactions on Pattern Analysis and Machine Intelligence.* (1989).

[12] Harten, A. Multiresolution algorithms for the numerical solution of hyperbolic conservation laws. *Communication on Pure and Applied Mathematics.* (1995) **48**:1305-1342.

[13] Cohen, A., Kaber, S.M. and Postel, M. Adaptive multiresolution for finite volume solutions of gas dynamics. *Computers and Fluids.* (2003) **32**:31-38.

[14] Rouby, C., Rémond, D. and Argoul, P. Orthogonal polynomials or wavelet analysis for mechanical system direct identification. *Annals of Solid and Structural Mechanics.* (2009) **1**:41-58.

[15] Mallat, S. *A wavelet tour of signal processing.* Academic Press (2008).